Chinese Journal of Catalysis 35 (2014) 159–167

available at www.sciencedirect.com

ScienceDirect

journal homepage: www.elsevier.com/locate/chnjc

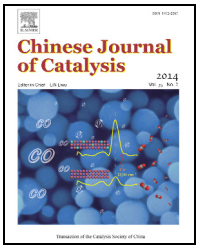

Article

The effect of doping transition metal oxides on copper manganese oxides for the catalytic oxidation of CO

Lina Cai [a], Zhenhao Hu [a], Peter Branton [b], Wencui Li [a,*]

[a] *State Key Laboratory of Fine Chemicals, Department of Chemical Engineering, Dalian University of Technology, Dalian 116024, Liaoning, China*
[b] *Group Research and Development, British American Tobacco, Regents Park Road, Millbrook, Southampton SO15 8TL, UK*

ARTICLE INFO

Article history:
Received 27 July 2013
Accepted 2 September 2013
Published 20 February 2014

Keywords:
Copper manganese oxide
Transition metal oxide
Doping
Carbon monoxide oxidation
Diffuse reflectance infrared Fourier transform spectroscopy

ABSTRACT

A series of copper manganese oxides doped with transition metal oxides were prepared by co-precipitation using copper acetate and manganese acetate as precursors, ammonium bicarbonate as precipitant, and metal nitrates as dopants. The catalysts were characterized by N_2 adsorption-desorption, X-ray powder diffraction, temperature-programmed reduction, and in situ diffuse reflectance infrared Fourier transform spectroscopy. The results showed that doping transition metal oxides into copper manganese oxides can modify the CO adsorption ability of the catalyst and thus affect the catalytic oxidation of CO.

1. Introduction

Catalytic oxidation of CO is one of the most effective methods of CO removal at low temperatures and has received considerable attention because of its many applications in industry and environmental fields. These include personal respiratory protective devices, CO_2 laser gas generation, proton exchange membrane fuel cells, and automobile emission controls [1–6]. Compared with noble metal catalysts, non-noble metal oxide catalysts have the advantages of high availability and low cost. Among them, hopcalite based on manganese-copper mixed oxide, a well-known catalyst for CO oxidation, has attracted attention because of its low price and relatively high catalytic activity. However, it has poor low-temperature catalytic activity and moisture resistance [7–9].

More recently, many attempts have been made to improve the catalytic activity of copper manganese oxides for CO oxidation, in particular by optimizing the preparation technologies and the improvement of preparation methods [7–20]. Among these methods, doping a transition metal oxide into the copper manganese oxide catalysts could tune the oxygen mobility and the reduction ability of the catalysts, thus improving the catalytic activity. It was found that after doping a small amount of CeO_2 into copper manganese oxide, a highly dispersed CeO_2 phase could prevent sintering and aggregating of the catalyst. In addition, the reducibility was enhanced, the particle size was decreased, and the formation of the active sites for the oxidation of CO was improved significantly. Therefore, the activity of this rare earth-promoted catalyst was enhanced remarkably [7]. It was also reported that copper manganese oxide catalysts, prepared by co-precipitation, had improved O^{2-} availability in the lattice and an enhanced surface area. By adding low levels

* Corresponding author. Tel/Fax: +86-411-84986355; E-mail: wencuili@dlut.edu.cn
This work was supported by the Fudamental Resarch Funds for the Central Universities (DUT12ZD218) and the Specialized Research Fund for the Doctoral Program of Higher Education (20100041110017).
DOI: 10.1016/S1872-2067(12)60699-8 | http://www.sciencedirect.com/science/journal/18722067 | Chin. J. Catal., Vol. 35, No. 2, February 2014

(~1.0 wt%) of Co, these materials can display much higher activity for CO oxidation compared with the current commercial copper manganese oxide catalysts at ambient conditions [8].

In our previous work [20], the combination effect of precipitant and precursor in the preparation has been studied. The precipitant shows the greatest influence on the crystalline phases of the catalyst while the precursor shows a greater effect on the number of catalytic active sites, both of which are directly related to the CO oxidation activity. In the present study, to further improve the catalytic activity of copper manganese oxide, we have prepared copper manganese oxide catalysts via co-precipitation by doping with transition metal oxides with (FeO_x or CeO_2) or without (ZnO) oxygen storage capacity. This study focuses on the influences of doping different transition metal oxide on CO adsorption and the resulting performance of the copper manganese oxide catalysts.

2. Experimental

2.1. Catalyst preparation

All chemicals used in this study were of analytical grade and used without further purification. The copper manganese oxide catalysts were prepared by co-precipitation using NH_4HCO_3 as the precipitant, the acetates of the copper and manganese as the precursors, and $Fe(NO_3)_3$, $Ce(NO_3)_3$, and $Zn(NO_3)_2$ as dopant. The typical procedure to synthesize the catalysts was as follows. A precipitant (30 mmol) was dissolved in deionized water (30 mL) with an initial pH value of *ca.* 8. The precursors (7.5 mmol) were mixed with deionized water (30 mL) with a 1/2 molar ratio of copper to manganese species. The mixed precursor solution was then added to the precipitant solution at 298 K with vigorous stirring. The resultant suspensions were aged for 30 min with continued vigorous stirring at 25 °C. Finally the precipitate was filtered, washed with deionized water and anhydrous alcohol, dried in air at 50 °C for 24 h, and then calcination at 300 °C for 2 h (denoted as $CuMO_x$-M, M = Fe, Zn, Ce) to obtain the final catalysts. The content of the doping transition metal oxide was fixed at 5 wt%. For comparison, the pure copper oxide and manganese oxide catalysts were prepared separately using the acetate as the precursor and NaOH as the precipitant, and keeping the other synthesis and after-treatment conditions the same as the copper manganese oxides. The corresponding samples were named CuO and MnO_x, respectively.

2.2. Catalyst characterization

X-ray diffraction patterns (XRD) were obtained with a Rigaku D/MAX-2400 diffractometer using Cu K_α radiation (40 kV, 100 mA, λ = 1.54056 Å). The textural characterizations of the samples were performed by nitrogen sorption at –196 °C using a Micromeritics Instrument Corporation Tristar 3000 device. Approximately 200 mg of the samples were heated to 200 °C under vacuum for 4 h to remove all adsorbed species. The surface area (S_{BET}) and pore size distribution were calculated using the BET method and BJH method, respectively. The total pore volume (V_{total}) was estimated from the amount adsorbed at a relative pressure of 0.99. The micropore volume was determined using the *t*-plot method. The morphologies of the catalysts were characterized with a FEI Quanta 450 instrument microscope equipped with a cooled energy-dispersive X-ray (EDX) spectrometer from Oxford Instruments for point-resolved elemental analysis. Hydrogen temperature programmed reduction (H_2-TPR) was performed by passing 8% H_2/Ar (50 mL/min) over a 20 mg sample (40–60 mesh size) at a heating rate of 10 °C /min to 900 °C. Before H_2-TPR, the samples were pretreated with Ar at 200 °C for 1 h. The system was then cooled to ambient temperature under Ar. The amount of hydrogen consumed (H_2 cons.) by each catalyst was calculated from the peak area of the H_2-TPR profile. In situ diffuse reflectance infrared Fourier transform spectra (DRIFTS) were recorded using a Nicolet 6700 FT-IR spectrometer at a resolution of 4 cm^{-1} from 4000 to 640 cm^{-1}. Self-supporting disks were prepared from the sample powders and treated directly in the IR cell. The catalysts were connected to a vacuum-adsorption apparatus with a residual pressure below 10^{-3} Pa. Prior to CO adsorption (5 vol% CO and N_2 in balance), the catalysts were evacuated for 30 min at 200 °C. After flushing with pure He for 10 min, the CO spectrum was collected again.

2.3. Catalytic test

The activity of the copper manganese oxide catalysts for CO oxidation was measured in a quartz tubular fixed-bed flow reactor at atmospheric pressure using 200 mg of catalyst (40–60 mesh). The standard composition of the feed gas was 1% CO, 20% O_2, and 79% N_2 with a space velocity (SV) of 20000 mL/(h·g_{cat}). The temperature was ramped to the final temperature at a rate of 1 °C/min. The concentrations of CO were analyzed at the outlet of the reactor by a Techcomp GC 7890T gas chromatograph equipped with a thermal conductivity detector. Temperatures for 100% conversion of CO ($T_{100\%}$) and 50% conversion of CO ($T_{50\%}$) were used to evaluate the activity of the catalysts. Long-term stability test of the $CuMnO_x$-Fe sample was conducted under atmosphere 30 °C, and SV = 20000 mL/(h·g_{cat}).

3. Results and discussion

3.1. Structure analyses of copper manganese oxides

XRD analysis was used to determine the final phase of the copper manganese oxide catalysts doped with different metal oxides after heat treatment at 300 °C in static air for 2 h (Fig. 1). It can be seen that the main crystal phase composition of the catalysts are Mn_2O_3, CuO, and $Cu_{0.139}Mn_{0.861}O_2$ with lower crystallinity. The crystal phase composition of the catalysts did not change significantly by doping with transition metal oxides, indicating that this addition does not significantly alter the bulk composition of the catalyst. Moreover, the characteristic diffraction peaks of the doped transition metal or any derivative did not appear due to low doping contents (below 5 wt%) or

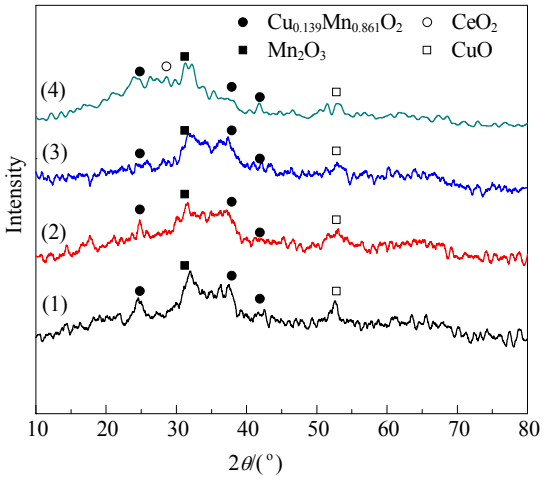

Fig. 1. XRD patterns of the copper manganese oxide catalysts. (1) $CuMnO_x$; (2) $CuMnO_x$-Fe; (3) $CuMnO_x$-Zn; (4) $CuMnO_x$-Ce.

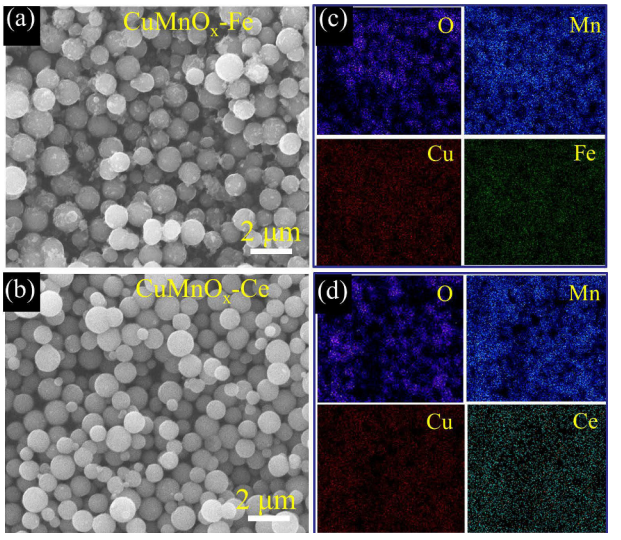

Fig. 3. SEM images of the catalysts. (a) $CuMnO_x$-Fe; (b) $CuMnO_x$-Ce; (c) Mapped results of $CuMnO_x$-Fe; (d) Mapped results of $CuMnO_x$-Ce.

highly dispersed or into the copper manganese oxide crystals lattice forming a solid solution [21].

Figure 2 shows the N_2 adsorption-desorption isotherms and the corresponding pore size distributions of the copper manganese oxide catalysts doped with different transition metal oxides. All the samples showed the typical mesoporous structure, which illustrated IV type isotherms with a hysteresis loop at relative pressures (p/p_0) of 0.4–0.8. The pore sizes of $CuMnO_x$, $CuMnO_x$-Zn, and $CuMnO_x$-Ce catalysts were mainly concentrated at 4.5 nm, and $CuMnO_x$-Fe at 2.7 nm. The specific surface area and the total pore volume of $CuMnO_x$, $CuMnO_x$-Fe, and $CuMnO_x$-Zn were similar. But these of $CuMnO_x$-Ce were decreased slightly. These characterizations demonstrated that the specific surface area, pore structure, and phase structure of copper and manganese oxide catalysts were only slightly affected by doping with transition metal oxides.

Figure 3 shows the SEM images and corresponding EDX elemental mapping images of the $CuMnO_x$-Fe and $CuMnO_x$-Ce catalysts. The obtained catalysts showed a sphere morphology with diameters of 0.5–1.5 μm. The elemental mapping images showed that the doped catalysts contained the expected elements (Fe, Ce). The Fe and Ce species were evenly distributed in the obtained catalysts, revealing that the transition metal oxide could be doped into copper manganese oxide during the co-precipitation process.

3.2. *Catalytic performance of the copper manganese oxides for CO oxidation*

Figure 4 displays the catalytic performance of the obtained catalysts for CO oxidation, and the corresponding activity is listed in Table 1. As shown in Fig. 4(a), the catalytic activity of all the catalysts increased as the reaction temperature and the activity towards CO oxidation strongly depends on the doped transition metal oxide, in the order $CuMnO_x$-Fe > $CuMnO_x$-Ce >

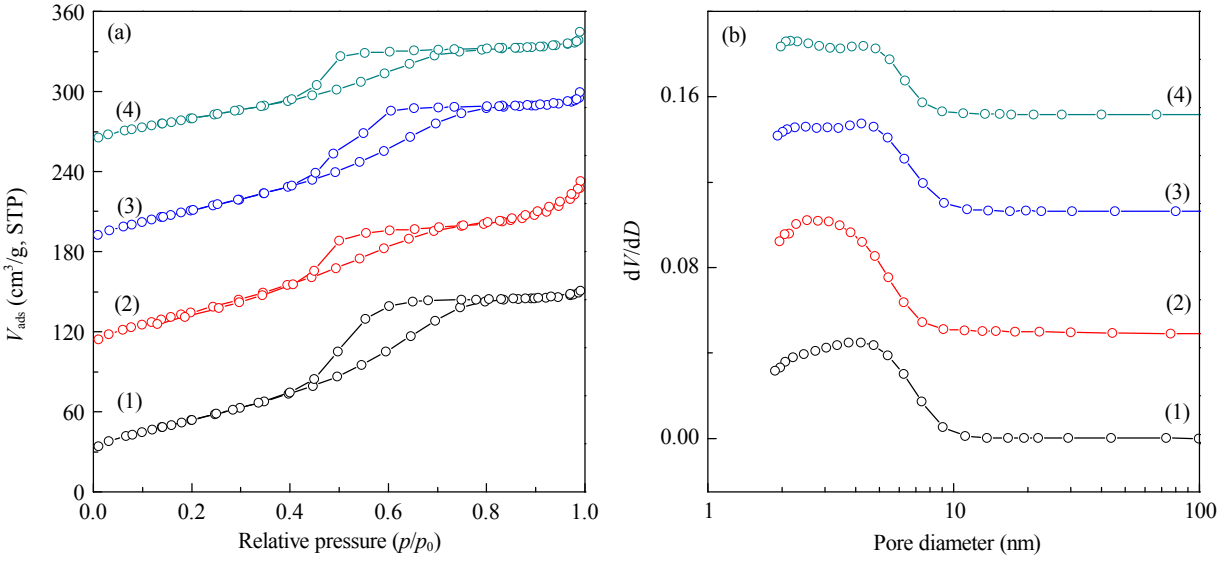

Fig. 2. N_2 adsorption-desorption isotherms (a) and pore size distributions (b) of the copper manganese oxide catalysts. (1) $CuMnO_x$; (2) $CuMnO_x$-Fe; (3) $CuMnO_x$-Zn; (4) $CuMnO_x$-Ce. Curves (2), (3), and (4) in (a) offset vertically by 80, 160, and 240 cm^3/g, STP, respectively.

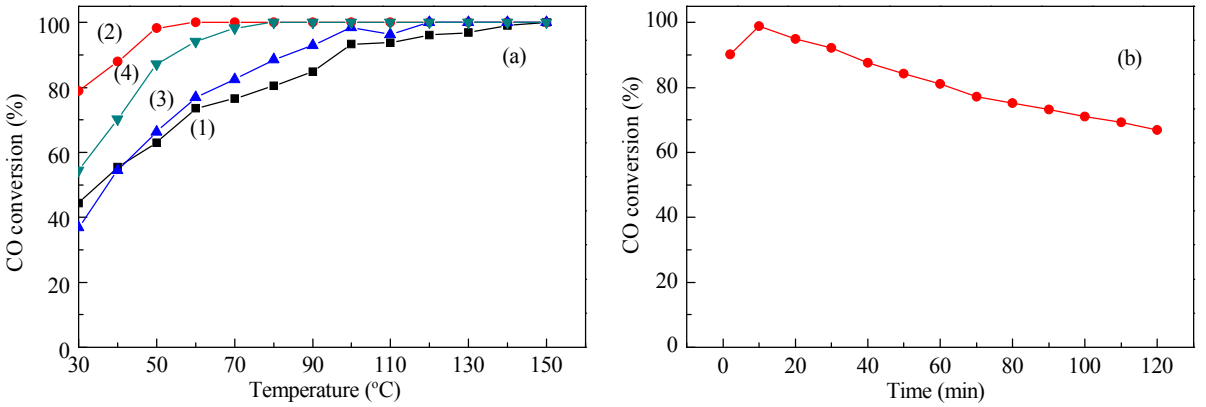

Fig. 4. (a) Catalytic activity of copper manganese oxides $CuMnO_x$ (1), $CuMnO_x$-Fe (2), $CuMnO_x$-Zn (3), and $CuMnO_x$-Ce (4) for CO oxidation. (b) Long-term stability of $CuMnO_x$-Fe at 30 °C.

$CuMnO_x$-Zn > $CuMnO_x$. The $CuMnO_x$ catalyst without doping showed 44% of CO conversion at 30 °C and achieved complete conversion ($T_{100\%}$) at 140 °C. Although there was no obvious improvement on the catalytic activity of $CuMnO_x$-Zn catalyst at 30 °C, the complete conversion temperature of CO shifted to 100 °C, exhibiting higher catalytic activity than that of $CuMnO_x$ catalyst. The improvement in the catalytic activity of $CuMnO_x$-Ce sample was due to the ability of the included Ce to enhance the oxygen storage capacity and oxygen mobility in the catalysts [5]. The CO conversion over $CuMnO_x$-Fe catalyst at 30 °C was raised by 35% compared with the $CuMnO_x$ catalyst, and this catalyst was able to achieve a complete conversion at 60 °C.

Table 1
Textural parameters and catalytic activity of the copper manganese oxide catalysts.

Sample	S_{BET} [a] (m^2/g)	V_{total} [b] (cm^3/g)	$C_{30°C}$ [c] (%)	$T_{100\%}$ [d] (°C)
$CuMnO_x$	196	0.23	44	140
$CuMnO_x$-Fe	199	0.24	79	60
$CuMnO_x$-Zn	185	0.22	37	100
$CuMnO_x$-Ce	145	0.16	54	80

[a] Specific surface area calculated by the BET method.
[b] Total pore volume calculated by the amount adsorbed at a relative pressure of 0.99.
[c] CO conversion at 30 °C.
[d] Temperature at complete conversion of CO to CO_2.

This remarkable improvement in the catalytic activity could be attributed to the increase in defects, formed by doping with ferric oxide, which improves the adsorption of the reactants, CO and O_2 [8].

Furthermore, a long-term stability test (Fig. 4(b)) of a $CuMnO_x$-Fe sample was conducted under reaction atmosphere at 30 °C with a space rate of 20000 mL/(h·g_{cat}). The CO conversion gradually decreased with time and reached about 65% after 120 min.

3.3. Reduction properties of copper manganese oxides catalysts and doped catalysts

Figure 5 gives H_2-TPR profiles of fresh calcined samples. The obtained catalysts showed three asymmetric reduction peaks except for the $CuMnO_x$-Fe catalyst (four reduction peaks). The corresponding fitted H_2-TPR profiles were also shown in Fig. 5. The fitted data and the H_2 consumption data calculated from the integration of the corresponding peak areas are listed in Table 2. For $CuMnO_x$, the reduction peaks at 141.9 and 164.9 °C could be assigned to the step reductions of $CuO \rightarrow Cu_2O \rightarrow Cu$, which were significantly lower than the reported in the literature [22]. This illustrated that the reducibility of Cu species could be improved by the interaction between Cu and Mn species. Another two fitted peaks at higher temperature could be attributed to the step reduction of $Mn_2O_3 \rightarrow Mn_3O_4 \rightarrow MnO$ [15].

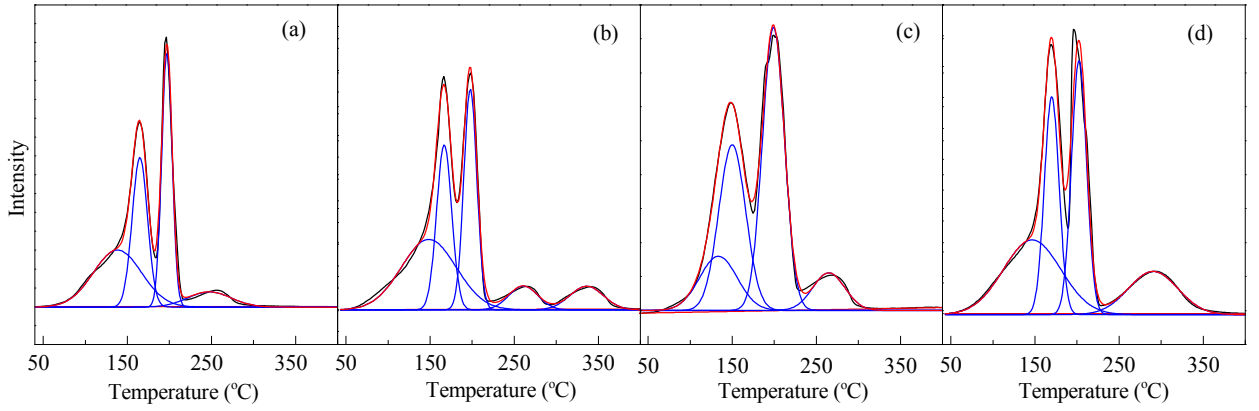

Fig. 5. H_2-TPR profiles of the copper manganese oxide catalysts. (a) $CuMnO_x$; (b) $CuMnO_x$-Fe; (c) $CuMnO_x$-Zn; (d) $CuMnO_x$-Ce.

Table 2
H_2-TPR fitted results of the copper manganese oxide catalysts.

Sample	CuO		MnO_x		Others	
	T/°C	H_2 consumption (cm^3/g)	T/°C	H_2 consumption (cm^3/g)	T/°C	H_2 consumption (cm^3/g)
$CuMnO_x$	141.9, 164.9	103.8	197.1, 247.6,	67.8	—	—
$CuMnO_x$-Fe	148.4, 166.8	100.4	197.8, 260.8	56.2	336.1	12.5
$CuMnO_x$-Zn	133.6, 150.0	59.5	199.0, 264.8	68.3	—	—
$CuMnO_x$-Ce	146.6, 169.9	86.0	202.4, 290.5	68.5	—	—

The TPR patterns of $CuMnO_x$-Zn and $CuMnO_x$-Ce were similar to $CuMnO_x$. However, there are four peaks over $CuMnO_x$-Fe. The fourth reduction peak could be assigned to the reduction of FeO_x species [23,24]. Based on the integrated analysis of Figure 4 and Table 2, the reduction peak of the $CuMnO_x$-Zn catalyst shifted to lower temperature, demonstrating its enhanced reducibility. Moreover, the reduction peaks of $CuMnO_x$-Fe and $CuMnO_x$-Ce shifted to higher temperature and the hydrogen consumption amount decreased, confirming the decrease in the catalyst's reducibility.

3.4. CO adsorption ability of the copper manganese oxide catalysts

To further demonstrate the impact of doping transition metal oxide on the copper manganese oxide catalysts, in situ DRIFTS of the obtained samples was performed to study the CO adsorption behavior on the catalysts' surface. Pure CuO catalyst and MnO_x catalyst were also studied for comparison. As shown in Fig. 6, MnO_x showed three weak peaks, which can be assigned to CO weakly adsorbed on the Mn species, while CuO exhibited strong adsorption of CO centered at 2171, 2121, and 2055 cm^{-1}. The strong at 2121 cm^{-1} band was attributed to the linear adsorption of CO on Cu^+, which is the typical absorption mode on CuO catalysts [25,26]. The weaker bands at 2055 and 2171 cm^{-1} were assigned to the CO linearly adsorbed on Cu^0 [27] and Cu^{2+} [28], respectively. The liner CO adsorption peak on copper manganese oxide catalysts is red-shifted to 2110 cm^{-1}. This can be attributed to the strong interaction between copper oxide and manganese oxide, which in turn weakens the C≡O bond. After doping with a transition metal oxide, the Cu^+–CO adsorption peak of the catalysts does not change. This demonstrates that doping with transition metal oxide does not weaken the interaction between copper and manganese oxides. However, the intensity of the adsorption peak is enhanced, indicating that the number CO adsorption sites increases. The intensity of the vibrational absorption peak at 2110 cm^{-1} was ordered $CuMnO_x$-Fe > $CuMnO_x$-Ce > $CuMnO_x$-Zn ≈ $CuMnO_x$. Combined with the H_2-TPR results, doping with Fe or Ce oxides could promote the interaction between the copper and manganese oxides, and this enhanced the Cu^{2+}→Cu^+ reduction. By increasing the Cu^+ content, the CO adsorption capacity of the catalyst is increased significantly. The CO adsorption capacity of the zinc oxide catalyst was the same as the copper manganese catalyst, which is consistent with the catalytic activity data.

Figure 7 shows the in situ DRIFTS spectra of catalysts adsorbed CO at 25 °C at different time intervals. The $CuMnO_x$-Fe

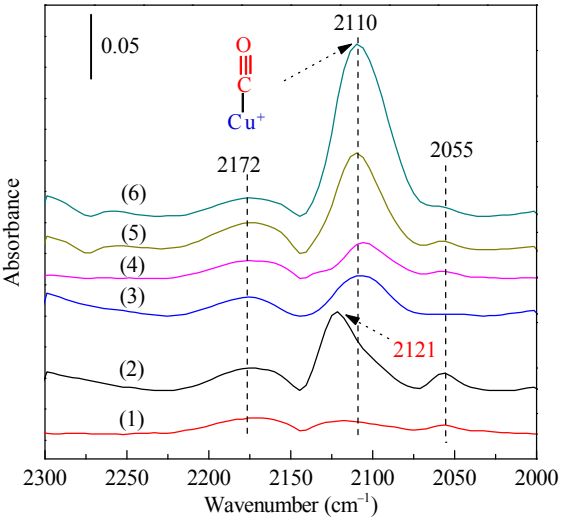

Fig. 6. DRIFTS spectra of CO adsorbed on the catalysts after 20 min at 25 °C. (1) MnO_x; (2) CuO; (3) $CuMnO_x$; (4) $CuMnO_x$-Zn; (5) $CuMnO_x$-Ce; (6) $CuMnO_x$-Fe.

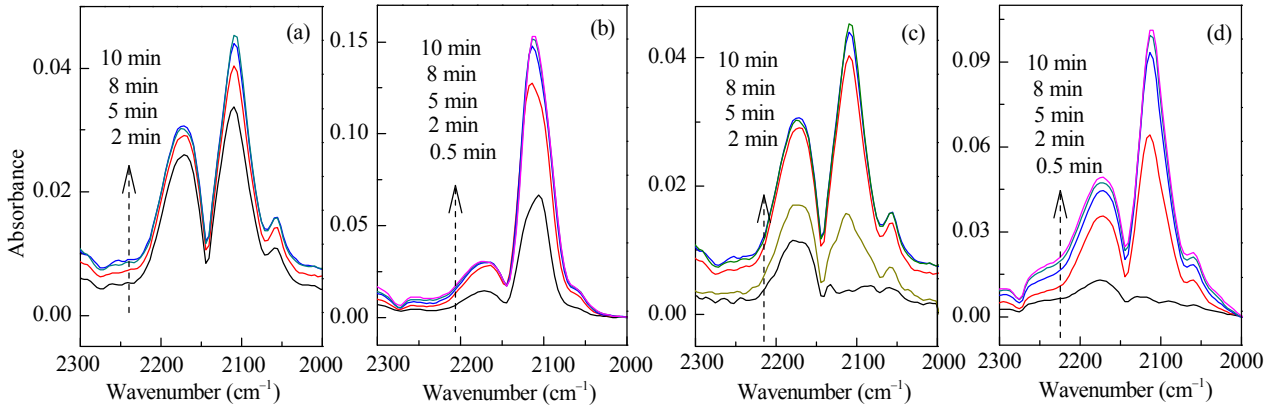

Fig. 7. DRIFTS spectra of the catalysts adsorbed CO at 25 °C at different time intervals. (a) $CuMnO_x$; (b) $CuMnO_x$-Fe; (c) $CuMnO_x$-Zn; (d) $CuMnO_x$-Ce.

Graphical Abstract

Chin. J. Catal., 2014, 35: 159–167 doi: 10.1016/S1872-2067(12)60699-8

The effect of doping transition metal oxides on copper manganese oxides for the catalytic oxidation of CO

Lina Cai, Zhenhao Hu, Peter Branton, Wencui Li *
Dalian University of Technology, China;
British American Tobacco, UK

Doping with specific transition metal oxides can enhance the CO adsorption on Cu^+ in a copper manganese oxide catalyst and benefits its catalytic oxidation.

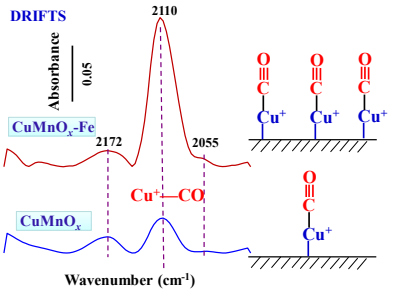

catalysts show a strong adsorption of CO occurred at 2 min while the adsorption of CO was complete at 5 min; the other catalyst generally required about 8–10 min before reaching saturation. This implies that $CuMnO_x$-Fe can adsorb CO quickly during the reaction, thereby increasing the catalytic activity.

4. Conclusions

Copper manganese oxide catalysts doped with Fe, Ce, and Zn oxides were prepared via co-precipitation. The addition of iron oxide and cerium oxide increase oxygen storage capacity of the copper manganese oxide catalysts, and can significantly improve CO adsorption capacity, and thus the performance of CO oxidation. Zinc oxide with no oxygen storage capacity, can increase the reduction performance of copper manganese oxide catalyst and improve the catalytic activity for CO oxidation. Catalytic tests showed that the $CuMnO_x$-Fe exhibited excellent catalytic performance with a 30%–40% enhancement in the CO conversion at 30 °C and total oxidation of CO can be achieved at 60 °C.

References

[1] Feng Y F, Wang L, Zhang Y H, GuoY, Guo Y L, Lu G Z. *Chin J Catal*, 2013, 34: 923
[2] Frey K, Iablokov V, Sáfrán G, Osán J, Sajó I, Szukiewicz R, Chenakin S, Kruse N. *J Catal*, 2012, 287: 30
[3] Yu Y B, Takei T, Ohashi H, He H, Zhang X L, Haruta M. *J Catal*, 2009, 267: 121
[4] Biabani A, Rezaei M, Fattah Z. *J Nat Gas Chem*, 2012, 21: 415
[5] Zhang R R, Ren L H, Lu A H, Li W C. *Catal Commun*, 2011, 13: 18
[6] Zhang H P, Liu H C. *J Energy Chem*, 2013, 22: 98
[7] Zhang X B, Ma K Y, Zhang L H, Yong G P, Dai Y, Liu S M. *Chin J Chem Phys*, 2011, 24: 97
[8] Jones C, Taylor S H, Burrows A, Crudace M J, Kiely C J, Hutchings G J. *Chem Commun*, 2008: 1707
[9] Li X Q, Xu J, Zhou L P, Gao J, Wang F, Chen C. *Chin J Catal*, 2006, 5: 369
[10] Morales M R, Barbero B P, Cadús L E. *Appl Catal B*, 2006, 67: 229
[11] Mirzaei A A, Shaterian H R, Joyner R W, Stockenhuber M, Taylor S H, Hutchings G J. *Catal Commun*, 2003, 4: 17
[12] Mirzaei A A, Shaterian H R, Habibi M, Hutchings G J, Taylor S H. *Appl Catal A*, 2003, 253: 499
[13] Hutchings G J, Mirzaei A A, Joyner R W, Siddiqui M R H, Taylor S H. *Appl Catal A*, 1998, 166: 143
[14] Li J, Zhu P F, Zhou R X. *J Power Sources*, 2011, 196: 9590
[15] Njagi E C, Chen C H, Genuino H, Galindo H, Huang H, Suib S L. *Appl Catal B*, 2010, 99: 103
[16] Tang Z R, Jones C D, Aldridge J K W, Davies T E, Bartley J K, Carley A F, Taylor S H, Allix M, Dickinson C, Rosseinsky M J, Claridge J B, Xu Z L, Crudace M J, Hutchings G J. *ChemCatChem*, 2009, 1: 247
[17] Hasegawa Y I, Maki R U, Sano M, Miyake T. *Appl Catal A*, 2009, 371: 67
[18] Liu Q, Wang L C, Chen M, Liu Y M, Cao Y, He H Y, Fan K N. *Catal Lett*, 2008, 121: 144
[19] Fortunato G, Oswald H R, Reller A. *J Mater Chem*, 2001, 11: 905
[20] Cai L N, Guo Y, Lu A H, Branton P, Li W C. *J Mol Catal A*, 2012, 360: 35
[21] Li J, Zhu P F, Zuo S F, Huang Q Q, Zhou R X. *Appl Catal A*, 2010, 381: 261
[22] Solsona B, Garcia T, Agouram S, Hutchings G J, Taylor S H. *Appl Catal B*, 2011, 101: 388
[23] Khoudiakov M, Gupta M C, Deevi S. *Appl Catal A*, 2005, 291: 151
[24] Zieliński J, Zglinicka I, Znak L, Kaszkur Z. *Appl Catal A*, 2010, 381: 191
[25] Neophytides S G, Marchi A J, Froment G F. *Appl Catal A*, 1992, 86: 45
[26] Gott T, Oyama S T. *J Catal*, 2009, 263: 359
[27] Manzoli M, Monte R D, Boccuzzi F, Coluccia S, Kašpar J. *Appl Catal B*, 2005, 61: 192
[28] Gamarra D, Martínez-Arias A. *J Catal*, 2009, 263: 189